Computed Tomography Image Restoration Using a Quantum-Based Deep Unrolled Denoiser and a Plug-and-Play Framework

Sayantan Dutta*‡†, Kenule Tuador Nwigbo*, Jérôme Michetti*, Bertrand Georgeot‡,
Duong Hung Pham*, Denis Kouamé*, Adrian Basarab†

*Institut de Recherche en Informatique de Toulouse, CNRS UMR 5505, Université de Toulouse, France
‡Laboratoire de Physique Théorique, Université de Toulouse, CNRS, UPS, France
†Université de Lyon, INSA-Lyon, UCBL, CNRS, Inserm, CREATIS UMR 5220, U1206, Villeurbanne, France

***Abstract*—In this work, we address the problem of cone beam computed tomography (CBCT) image resolution enhancement by exploiting a newly introduced deep unrolled quantum denoiser, based on quantum interaction theory adapted to computational imaging. Following recent advances in image restoration using the Plug-and-Play (PnP) framework, we impose this external deep learning denoiser as a regularizer within the super-resolution (SR) problem. The quantum-based deep unrolled denoiser combined with a computationally efficient way to deal with the degradation operators, and the PnP scheme, result in an original way of approaching the image resolution enhancement problem. Experiments conducted on dental CBCT images are presented to illustrate the efficiency of the proposed model for image resolution enhancement tasks. The numerical results suggest that the proposed method allows better restoration performances compared to existing state-of-the-art approaches.**

***Index Terms*—Super-Resolution, Plug-and-Play, Unrolling, Deep learning, Quantum denoising, DIVA, Quantum image processing.**

I. Introduction

Root canal treatment is a common procedure routinely performed by dentists to treat dental infections. Despite its increasing use in clinics, the success rate is only 60%–85% [1], [2] due to the low spatial resolution of dental computed tomography (CT) images leading to root canal-related endodontic therapeutic failure. Therefore, a better visualization of the internal structure of the root canal by enhancing spatial resolution in post-processing is an important factor in medical imaging. Estimating high-resolution (HR) images from low-resolution (LR) observations is a classical inverse problem known as super-resolution (SR). Traditional SR algorithms can be broadly classified into two categories: model-based [3]–[7] and learning-based approaches [8]–[12]. Recently, model-based deep learning (DL) algorithms [13]–[16] brought another alternative by combining the advantages of model- or learning-based methods. DL-aided models [17]–[19] are hybrid algorithms that use traditional model-based inference, hence improved using the power of convolutional neural network (CNN). The focus of this work is to design a new DL-aided scheme for SR problem by exploiting a quantum mechanics-based deep unrolled denoiser and a computational efficient way to deal with the decimation and blurring operators simultaneously by taking advantage of their underlying properties in the frequency domain.

In the last few years, algorithms based on quantum mechanics theory have been successfully applied in various image processing applications [20]–[24]. This work proposes a way of solving the SR problem by exploiting a newly introduced quantum-based DL denoiser [25], [26], hereafter denoted as DIVA (Deep denoising by quantum InteractiVe pAtches), which unrolled the baseline adaptive quantum denoising algorithm (De-QuIP) proposed in [22], [23]. DIVA inherently absorbs the idea of quantum interaction and Hamiltonian operator from De-QuIP [23], while efficiently exploiting the power of CNN architecture. More precisely, the quantum interactions preserve local similarity between neighboring patches, while convolution kernels efficiently solve the hyperparameter tuning problem. The main novelty of this work is (i) the integration of the deep unrolled denoiser into the DL-aided framework combined with a model-based analytical inference to handle the degradation operators and (ii) the experiments on dental CBCT images.

II. Proposed Deep Learning-Aided Super-Resolution Scheme

A. Problem Formulation

In the single image SR problem, the acquired image $\mathbf{y} \in \mathbb{R}^N$ is modeled as a LR observation of a noisy, blurry and decimated version of a hidden HR image $\mathbf{x} \in \mathbb{R}^{dN}$, mathematically expressed by

$$\mathbf{y} = \mathbf{S}\mathbf{H}\mathbf{x} + \mathbf{e}, \tag{1}$$

where $\mathbf{S} \in \mathbb{R}^{N \times dN}$ is the decimation operator, $\mathbf{H} \in \mathbb{R}^{dN \times dN}$ the blurring operator, assumed to be a block circulant matrix with circulant blocks (BCCB), $\mathbf{e} \in \mathbb{R}^N$ an additive white Gaussian noise (AWGN). Note that $\mathbf{y}$, $\mathbf{x}$ and $\mathbf{e}$ are column vectors representing images reshaped in classical lexicographic order.

Following a classic Bayesian framework, the maximum-a-posteriori (MAP) estimator expresses this highly ill-posed

estimation problem of the HR image from the observed LR data as the minimization of a cost function:

$$\hat{\mathbf{x}} = \arg\min_{\mathbf{x}} \; \frac{1}{2} \underbrace{\|\mathbf{SHx} - \mathbf{y}\|_2^2}_{\text{Data fidelity}} + \underbrace{\lambda g(\mathbf{x})}_{\text{Regularization}} \quad , \tag{2}$$

where $\hat{\mathbf{x}}$ is the restored HR image and λ is a hyper-parameter. The *data fidelity* term is quadratic under the Gaussian noise assumption, and the *regularization* term results from an *a priori* statistical distribution of the latent image $\mathbf{x}$. Thus, the optimal choice of this regularization term is crucial to obtain a reliable solution. The most common prior distributions exploited in the literature are based on the sparsity or piecewise smoothness of the HR image.

A breakthrough was made in the literature in the last decade, enabling the use of a state-of-the-art denoisers instead of an explicit regularization function by redefining the image restoration problem into a chain of denoising processes using the PnP framework [27], [28]. Over the past few years, numerous denoiser-based priors have been proposed, exploiting different mathematical tools, among which the non-local self-similarity (NLSS) [29], [30] is an extensively exploited property due to its promising image denoising performances. The PnP framework intelligently utilizes these advantages of the NLSS-based denoisers by integrating them as an underlying prior in the image restoration process [31]–[36].

Despite the success of these NLSS-based denoisers, their computational cost represents an important challenge amplified by their iterative use within the PnP framework. Furthermore, these external denoisers are associated with internal hyperparameters that are usually related to the level of noise, and need thus to be tuned at each iteration of the PnP scheme to obtain the best restoration result [18], [19]. Although it is possible to fix these hyperparameters based on some presumptions [18], [32], that choice is not optimal in most cases, particularly in medical imaging applications.

The CNN-based denoisers [37]–[39] mitigate these limitations by harnessing a large training dataset to learn the map between the noisy and latent images. In recent years, model-based DL (known as deep unrolling) architectures [40], [41] have been attracting increasingly attention due to their explanatory properties compared to traditional CNN-based models [37]–[39], while reducing the disadvantages of the model-based regularizers by exercising the power of back propagation. In this work, we exploit such a deep unrolled denoiser, denoted as DIVA [25], [26], inspired by the principles of quantum many-body physics, which acts as an implicit prior function in the PnP framework for solving the SR problem expressed in (1). The following subsections present the key concepts of the DIVA network architecture built on the baseline quantum-based De-QuIP algorithm [22], [23] and its implementation into a SR algorithm using the PnP scheme.

B. Quantum-Based Deep Unrolled DIVA Network for Denoising

Built on an underlying many-body quantum theory, DIVA consists in a deep denoising network by unrolling the baseline De-QuIP algorithm initially proposed in [23]. The many-body quantum theory deals with more than one quantum particle, where interactions between particles inevitably arise. De-QuIP exploits this theory of interactions and extends this concept to imaging problems by dividing an image into small patches, where every image patch behaves like a single-particle system and interacts with neighboring patches similar to a many-body system. These interactions exploit the NLSS between neighboring patches that significantly enhance the denoising performance of De-QuIP by updating the adaptive wave functions used for the patch decomposition. These adaptive wave functions, the solutions of the Schrödinger equation, *i.e.*, the eigenvectors of the respective Hamiltonian operator, characterize the values of different image pixels using different level frequency bands. We refer readers to the seminal works [21]–[23] for more details about these adaptive wave functions and the De-QuIP algorithm.

DIVA proposes a CNN network while preserving the core philosophies of the De-QuIP framework. Indeed, to enrich the adaptive nature of the baseline algorithm, patch-based computations with fixed hyperparameters are replaced by convolutional layers. Furthermore, harnessing the power of backpropagation, the unrolled DIVA network efficiently solves the hyperparameter tuning problem associated with its baseline De-QuIP algorithm [25], [26]. The DIVA network architecture is primarily composed of seven main layers. The first layer extracts all patches from the noisy input image and creates their respective local neighboring groups. The next layer computes the total interaction for each local group using a convolution operation followed by Rectified Linear Unit (ReLU) function. The ReLU is used to trim any redundant contributions to interactions. Following the baseline algorithm, DIVA constructs a Hamiltonian kernel $\boldsymbol{C}_{2_a} = \boldsymbol{K}_a\nabla^2 + \boldsymbol{J}_a + \boldsymbol{I}_a$ for the a-th patch, where $\boldsymbol{K}_a$, $\boldsymbol{J}_a$ and $\boldsymbol{I}_a$ are respectively a learnable kernel associated with hyperparameters, noisy patch/original potential, and the total interaction computed in the previous layer. This Hamiltonian kernel plays a role in the next convolutional layer to get the projection coefficients. Note that the gradient operator ∇ does not change during the training process to preserve the quantum principles of the original De-QuIP. Next, thresholding is done by a nonlinear ReLU activation function, and a convolution operation with a learnable kernel is used to obtain denoised patches. Finally, by accumulating all restored patches in the aggregation layer, DIVA recovers the denoised image. Note that the exploitation of a quantum-based deep unrolled denoiser is highly original in this context. For more detailed mathematical construction of DIVA, the reader may refer to the recent works [25], [26], [42].

C. Plug-and-Play SR Algorithm Using Deep Unrolled DIVA

One common way to solve SR problems is to use an iterative convex optimization algorithm, *e.g.*, alternate direction method of multipliers (ADMM) [6]. Under the umbrella of ADMM, PnP provides an elegant way to decompose the restoration task (2) into two subproblems of image denoising coupled with an inverse task, where an off-the-shelf denoiser tackles the

denoising step separately [32]. The most interesting feature of PnP is that there is no need to specify an explicit regularization function $g(\mathbf{x})$, rather a mutual dependence exists between the regularization and off-the-shelf denoising operator $\mathcal{D}$ intrinsically.

With appropriate parameterization, ADMM can be used to reformulate the MAP estimator (2) into the following constrained-based optimization problem:

$$\hat{\mathbf{x}} = \frac{1}{2}\arg\min_{\mathbf{x}} \quad \|\mathbf{SHx} - \mathbf{y}\|_2^2 + \lambda g(\mathbf{v}), \quad \text{s.t.} \quad \mathbf{x} = \mathbf{v}, \tag{3}$$

with an associated augmented Lagrangian function,

$$\mathcal{L}_{(\mathbf{x},\mathbf{v},\mathbf{u})} = \frac{1}{2}\|\mathbf{SHx} - \mathbf{y}\|_2^2 + \lambda g(\mathbf{v}) + \frac{\beta}{2}\|\mathbf{x} - \mathbf{v} + \mathbf{u}\|_2^2, \tag{4}$$

where β and $\mathbf{u}$ are respectively a hyperparameter and the Lagrangian multipliers. After variable splitting, the problem (4) can be solved iteratively as:

$$\mathbf{v}^{k+1} = \arg\min_{\mathbf{v}} \quad \lambda g(\mathbf{v}) + \frac{\beta}{2}\left\|\mathbf{x}^k - \mathbf{v} + \mathbf{u}^k\right\|_2^2, \tag{5a}$$

$$\mathbf{x}^{k+1} = \arg\min_{\mathbf{x}} \|\mathbf{SHx} - \mathbf{y}\|_2^2 + \frac{\beta}{2}\left\|\mathbf{x} - \mathbf{v}^{k+1} + \mathbf{u}^k\right\|_2^2, \tag{5b}$$

$$\mathbf{u}^{k+1} = \mathbf{u}^k + \mathbf{x}^{k+1} - \mathbf{v}^{k+1}. \tag{5c}$$

One may notice that eq. (5a) can be rewritten as,

$$\mathbf{v}^{k+1} = \arg\min_{\mathbf{v}} \quad \lambda g(\mathbf{v}) + \frac{\beta}{2}\left\|\mathbf{v} - (\mathbf{x}^k + \mathbf{u}^k)\right\|_2^2, \tag{6}$$

which is actually a denoising algorithm assuming $g(\mathbf{v})$ a prior on the noisy image $(\mathbf{x}^k + \mathbf{u}^k)$. Hence, as already mentioned above, PnP formulation gives us the freedom to integrate the deep unrolled denoiser DIVA for solving eq. (5a) (or eq. (6)) without any explicit *prior* construction, this leads to

$$\mathbf{v}^{k+1} = \mathcal{D}\big(\mathbf{x}^k + \mathbf{u}^k\big), \tag{7}$$

where $\mathcal{D}$ is the symbolic notation for DIVA. Moving to eq. (5b), that is called data fitting subproblem, it has a closed-form solution

$$\mathbf{x}^{k+1} = \Big(\mathbf{H}^H\mathbf{S}^H\mathbf{SH} + \beta\mathbf{I}\Big)^{-1}\Big(\mathbf{H}^H\mathbf{S}^H\mathbf{y} + \beta(\mathbf{v}^{k+1} - \mathbf{u}^k)\Big). \tag{8}$$

Under the cyclic boundary assumption, the blurring operator $\mathbf{H}$ and its conjugate transpose $\mathbf{H}^H$ are diagonalizable in Fourier domain as, $\mathbf{H} = \mathbf{F}^H\mathbf{\Lambda}\mathbf{F}$ and $\mathbf{H}^H = \mathbf{F}^H\mathbf{\Lambda}^H\mathbf{F}$, where the matrices $\mathbf{F}$ and $\mathbf{F}^H$ are respectively the Fourier and inverse Fourier transforms, and the diagonal matrix $\mathbf{\Lambda} = \text{diag}\{\mathbf{Fh}\}$, where $\mathbf{h}$ is the first column of $\mathbf{H}$. Here $\mathbf{S}^H$ and $\mathbf{I}$ are associated with the conjugate transpose of the decimation operator $\mathbf{S}$ and the identity matrix. For large-scale problems, the analytical solution of eq. (8) is not practical because of the non-diagonalizable nature of the operator $\mathbf{S}$, which restricts its efficient implementation in the Fourier domain. Traditional iterative optimization [4] and sampling [43] based computationally expensive algorithms are generally used to solve (8). However, the observations in [6] ensure the computationally efficient analytical solution for the eq. (8) in the Fourier domain by rewriting the (8) as

$$\mathbf{x}^{k+1} = \mathbf{F}^H\Big(\frac{1}{d}\underline{\mathbf{\Lambda}}^H\underline{\mathbf{\Lambda}} + \beta\mathbf{I}\Big)^{-1}\mathbf{F}\Big(\mathbf{H}^H\mathbf{S}^H\mathbf{y} + \beta(\mathbf{v}^{k+1} - \mathbf{u}^k)\Big), \tag{9}$$

where $\underline{\mathbf{\Lambda}} = [\mathbf{\Lambda}_1, \mathbf{\Lambda}_2, \cdots, \mathbf{\Lambda}_d] \in \mathbb{C}^{N\times dN}$, where the blocks $\mathbf{\Lambda}_j \in \mathbb{C}^{N\times N}$ for $j = 1, 2, \cdots, d$ satisfy $\text{diag}\{\mathbf{\Lambda}_1, \mathbf{\Lambda}_2, \cdots, \mathbf{\Lambda}_d\} = \mathbf{\Lambda}$. Lastly, the third step (5c) updates the Lagrangian multiplier. Hence, the proposed PnP-ADMM algorithm consists in three iterative steps (given by eqs. (7), (9) and (5c)) while exploiting quantum-based DIVA denoiser as the PnP denoising engine.

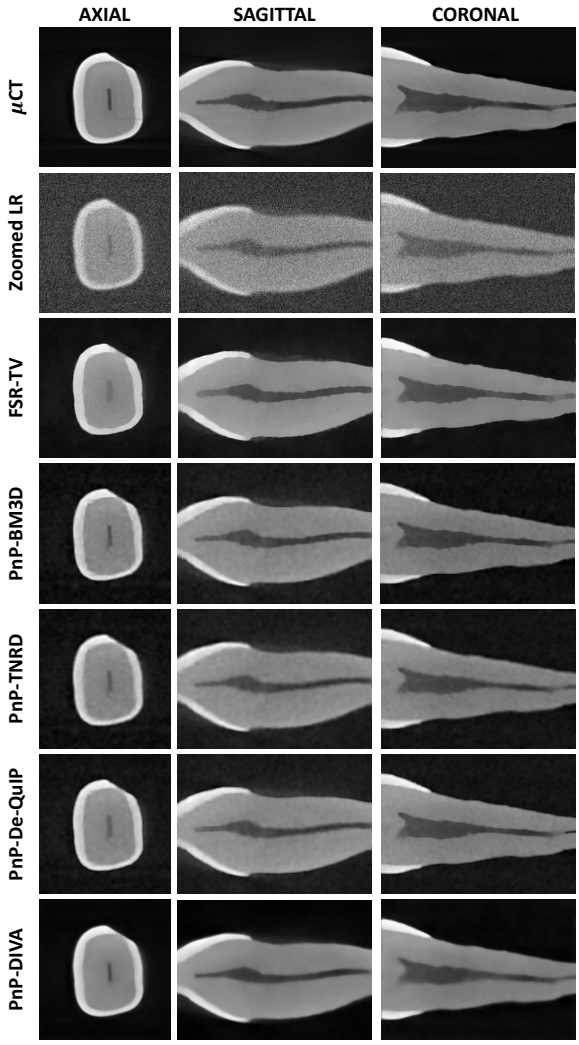

Fig. 1. Three restored tooth images from the μCT dataset containing 60 LR images. The dark region inside the tooth corresponds to the root canal.

III. Experimental Results

This section summarizes SR experiments conducted on dental CT datasets to illustrate the potential of the proposed PnP algorithm with DIVA, denoted by PnP-DIVA. In dental applications, cone beam CT (CBCT) imaging is often used for medical diagnosis due to its low exposure to X-ray doses. Hence, CBCT suffers from reduced spatial resolution and high level of noise, in particular for specific applications such

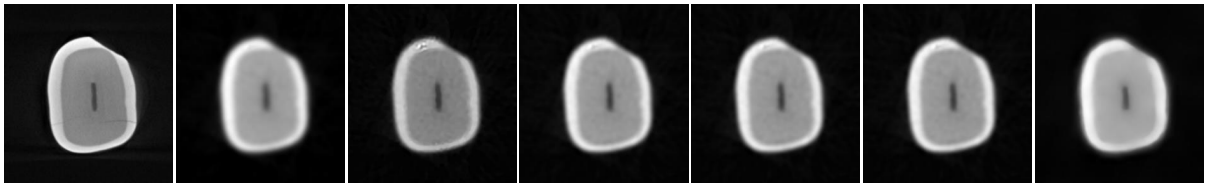

Fig. 2. One restored tooth image from the CBCT dataset. The dark region inside the tooth corresponds to the root canal.

as endodontics that concern the thin structure of root canal [1], [2]. On the other hand, μCT data provides high quality volumes, but only permits the imaging of extracted teeth because of the use of high radiation dose. Therefore, in this work, μCT is used to obtain the ground truth HR images. The first objective is to train the DIVA denoiser for CT images before moving toward the SR problems.

1) Training of DIVA: The DIVA network was trained in a supervised manner on a total of 500 μCT images (200 axial, 150 sagittal and 150 coronal slices) contaminated with AWGN with different signal-to-noise-ratios (SNRs). The model architecture was implemented in Keras and trained using NVIDIA GTX 1080 Ti GPU, with small batches of size 128 containing 40×40 patches, using the Adam optimizer with a learning rate that exponentially decays from 10^{-3} to 10^{-5} over 60 epochs. The mean squared error between the original and predicted residual is considered as the training loss [26].

2) Testing Datasets of PnP-DIVA: The first test dataset consists of 60 synthetic LR images (20 axial, 20 sagittal and 20 coronal slices) created from the μCT dataset using a 9×9 Gaussian smoothing kernel with standard deviation of 3, downsampling factors of 2 in each spatial direction, and an AWGN corresponding to blurred-signal-to-noise-ratio (BSNR) of 10 dB (Fig. 1). Within the second set of experiments, 60 CBCT images are used as LR image inputs, whose ground truths are not available directly. Hence, the respective μCT images acquired on the same tooth are considered as the HR data for the comparison perspective (Fig. 2). Note that the point spread function is unknown for the CBCT dataset, thus approximated for the axial, sagittal and coronal slices respectively by a Gaussian kernel with std 6.2, 0.4 and 3.3, by direct estimation from the CBCT data itself using the approach in [44].

3) Comparison methods: The proposed model is compared with four standard methods from the literature to illustrate its efficiency: i) a TV regularization based fast SR algorithm [6] denoted by FSR-TV, ii) the PnP algorithm using BM3D denoiser [27] denoted by PnP-BM3D, iii) PnP with the trainable nonlinear reaction diffusion (TNRD) denoiser [45], which uses a convolutional neural network-based flexible learning method for denoising, referred as PnP-TNRD, iv) PnP combined with the baseline De-QuIP algorithm as an external denoiser [46], denoted as PnP-De-QuIP.

4) Result Analysis: The resulting mean peak-signal-to-noise-ratio (PSNR) and structure similarity (SSIM) of the recovered μCT and CBCT images are regrouped in Table I. Quantitative data show that the proposed method provides better PSNR and SSIM matrices than existing state-of-the-art approaches. Furthermore, a notable gain is observed against the PnP-De-QuIP algorithm, which is a consequence of finely tuned hyperparameters in the DIVA model compared to its baseline De-QuIP scheme. Finally, the visual assessment of the restored HR μCT and SR CBCT images, respectively presented in Fig. 1 and Fig. 2, confirms the superiority of the proposed SR technique for enhancing the CBCT images, and especially to enhance the dark region of interest in the center of the tooth, corresponding to the root canal.

IV. Conclusion

This paper introduced a new SR algorithm that combines a quantum-based deep unrolled denoiser and an analytical solution for the inversion process. This deep unrolled denoiser DIVA takes advantage of quantum mechanical theory and exploits the powerful representation properties of DL networks. Integration of these key elements from two different branches of science increases the efficiency of the DIVA network while acting as a PnP prior in a SR problem. Experimental results on dental CT images demonstrated the restoration ability of our proposed PnP-DIVA scheme against benchmark techniques in SR CT imaging applications. As a continuation of this work, one can extend the proposed PnP scheme to the 3D SR problems or to non-Gaussian noise models, where a 3D extension of the DIVA network can be used for the regularization. Furthermore, the convergence analysis of such a PnP scheme under a deep unrolled denoiser is also interesting for future studies.

TABLE I
Quantitative SR results. The best values are in bold.

	Methods	Output	Tooth Image Slices		
			Axial	Sagittal	Coronal
μCT	FSR-TV	PSNR(dB)	33.61	34.26	34.25
		SSIM(%)	94.83	94.92	96.05
	PnP-BM3D	PSNR(dB)	34.40	35.48	35.61
		SSIM(%)	95.60	95.79	96.11
	PnP-TNRD	PSNR(dB)	34.67	35.72	35.21
		SSIM(%)	96.18	95.92	96.58
	PnP-De-QuIP	PSNR(dB)	34.65	35.89	35.25
		SSIM(%)	96.21	95.99	96.53
	PnP-DIVA	PSNR(dB)	**36.12**	**36.78**	**36.69**
		SSIM(%)	**97.84**	**98.12**	**97.95**
CBCT	FSR-TV	PSNR(dB)	22.59	22.43	23.70
		SSIM(%)	75.01	78.41	79.45
	PnP-BM3D	PSNR(dB)	22.53	22.75	23.67
		SSIM(%)	79.53	77.14	86.56
	PnP-TNRD	PSNR(dB)	22.52	23.31	23.78
		SSIM(%)	79.79	78.97	89.51
	PnP-De-QuIP	PSNR(dB)	22.47	22.85	23.77
		SSIM(%)	80.44	77.96	89.52
	PnP-DIVA	PSNR(dB)	**23.77**	**23.97**	**24.46**
		SSIM(%)	**82.27**	**79.36**	**90.78**

REFERENCES

[1] H.M. Eriksen, L.-L. Kirkevang, and K. Petersson, "Endodontic epidemiology and treatment outcome: General considerations," *Endodontic Topics*, vol. 2, no. 1, pp. 1–9, 2002.

[2] Y.-L. Ng, V. Mann, S. Rahbaran, J. Lewsey, and K. Gulabivala, "Outcome of primary root canal treatment: Systematic review of the literature–part 1. effects of study characteristics on probability of success," *Int. Endodontic J.*, vol. 40, no. 12, pp. 921–939, 2007.

[3] F. Shi, J. Cheng, L. Wang, P.-T. Yap, and D. Shen, "LRTV: MR image super-resolution with low-rank and total variation regularizations," *IEEE Trans. Med. Imag.*, vol. 34, no. 12, pp. 2459–2466, 2015.

[4] J. Sun, J. Sun, Z. Xu, and H.-Y. Shum, "Gradient profile prior and its applications in image super-resolution and enhancement," *IEEE Trans. Image Process.*, vol. 20, no. 6, pp. 1529–1542, 2011.

[5] J. Yang, J. Wright, T.S. Huang, and Y. Ma, "Image super-resolution via sparse representation," *IEEE Trans. Image Process.*, vol. 19, no. 11, pp. 2861–2873, 2010.

[6] N. Zhao, Q. Wei, A. Basarab, N. Dobigeon, D. Kouamé, and J.Y. Tourneret, "Fast single image super-resolution using a new analytical solution for $\ell_2 - \ell_2$ problems," *IEEE Trans. Image Process.*, vol. 25, no. 8, pp. 3683–3697, 2016.

[7] A. Beck and M. Teboulle, "A fast iterative shrinkage-thresholding algorithm for linear inverse problems," *SIAM J. Imag. Sci.*, vol. 2, no. 1, pp. 183–202, 2009.

[8] J. Hatvani, A. Horváth, J. Michetti, A. Basarab, D. Kouamé, and M. Gyöngy, "Deep learning-based super-resolution applied to dental computed tomography," *IEEE Trans. Radiat. Plasma Med. Sci.*, vol. 3, no. 2, pp. 120–128, 2019.

[9] C. Dong, C.C. Loy, K. He, and X. Tang, "Image super-resolution using deep convolutional networks," *IEEE Trans. Pattern Anal. Mach. Intell.*, vol. 38, no. 2, pp. 295–307, 2016.

[10] H. Chen, Y. Zhang, W. Zhang, P. Liao, K. Li, J. Zhou, and G. Wang, "Low-dose CT via convolutional neural network," *Biomedical Optics Express*, vol. 8, no. 2, pp. 679–694, 2017.

[11] J. Kim, J.K. Lee, and K.M. Lee, "Accurate image super-resolution using very deep convolutional networks," in *Proc. IEEE Conf. Comput. Vis. Pattern Recognit. (CVPR)*, 2016, pp. 1646–1654.

[12] Z. Wang, J. Chen, and S.C.H. Hoi, "Deep learning for image super-resolution: A survey," *IEEE Trans. Pattern Anal. Mach. Intell.*, vol. 43, no. 10, pp. 3365–3387, 2021.

[13] O. Solomon, R. Cohen, Y. Zhang, Y. Yang, Q. He, J. Luo, R.J.G. van Sloun, and Y.C. Eldar, "Deep unfolded robust PCA with application to clutter suppression in ultrasound," *IEEE Trans. Med. Imag.*, vol. 39, no. 4, pp. 1051–1063, 2020.

[14] K. Zhang, L.V. Gool, and R. Timofte, "Deep unfolding network for image super-resolution," in *Proc. IEEE Conf. Comput. Vis. Pattern Recognit. (CVPR)*, 2020, pp. 3217–3226.

[15] K.H. Jin, M.T. McCann, E. Froustey, and M. Unser, "Deep convolutional neural network for inverse problems in imaging," *IEEE Trans. Image Process.*, vol. 26, no. 9, pp. 4509–4522, 2017.

[16] N. Shlezinger, J. Whang, Y.C. Eldar, and A.G. Dimakis, "Model-based deep learning," *arXiv preprint arXiv:2012.08405*, 2020.

[17] E. Ryu, J. Liu, S. Wang, X. Chen, Z. Wang, and W. Yin, "Plug-and-play methods provably converge with properly trained denoisers," in *Proc. 36th Int. Conf. Machine Learning (ICML)*. PMLR, 2019, pp. 5546–5557.

[18] S. Kong, W. Wang, X. Feng, and X. Jia, "Deep red unfolding network for image restoration," *IEEE Trans. Image Process.*, vol. 31, pp. 852–867, 2022.

[19] K. Zhang, Y. Li, W. Zuo, L. Zhang, L. Van Gool, and R. Timofte, "Plug-and-play image restoration with deep denoiser prior," *IEEE Trans. Pattern Anal. Mach. Intell.*, vol. 44, no. 10, pp. 6360–6376, 2022.

[20] Ç. Aytekin, S. Kiranyaz, and M. Gabbouj, "Quantum mechanics in computer vision: Automatic object extraction," in *Proc. IEEE Int. Conf. Image Process. (ICIP)*, 2013, pp. 2489–2493.

[21] S. Dutta, A. Basarab, B. Georgeot, and D. Kouamé, "Quantum mechanics-based signal and image representation: Application to denoising," *IEEE Open J. of Signal Process.*, vol. 2, pp. 190–206, 2021.

[22] S. Dutta, A. Basarab, B. Georgeot, and D. Kouamé, "Image denoising inspired by quantum many-body physics," in *Proc. 28th IEEE Int. Conf. Image Process. (ICIP)*, 2021, pp. 1619–1623.

[23] S. Dutta, A. Basarab, B. Georgeot, and D. Kouamé, "A novel image denoising algorithm using concepts of quantum many-body theory," *Signal Processing*, vol. 201, pp. 108690, 2022.

[24] Y.-J. Xue, X.-J. Wang, J.-X. Cao, H.-K. Du, J.-Y. Xie, J.-C. You, X.-D. Jiang, and J. Yang, "Estimation of seismic quality factor via quantum mechanics-based signal representation," *IEEE Trans. Geosci. Remote Sens.*, vol. 60, pp. 1–11, 2022.

[25] S. Dutta, A. Basarab, B. Georgeot, and D. Kouamé, "Deep unfolding of image denoising by quantum interactive patches," in *Proc. IEEE Int. Conf. Image Process. (ICIP)*, 2022, pp. 491–495.

[26] S. Dutta, A. Basarab, B. Georgeot, and D. Kouamé, "DIVA: Deep unfolded network from quantum interactive patches for image restoration," *arXiv preprint arXiv:2301.00247*, 2022.

[27] S.V. Venkatakrishnan, C.A. Bouman, and B. Wohlberg, "Plug-and-play priors for model based reconstruction," in *Proc. IEEE Global Conf. Signal Inf. Process.*, 2013, pp. 945–948.

[28] U.S. Kamilov, C.A. Bouman, G.T. Buzzard, and B. Wohlberg, "Plug-and-play methods for integrating physical and learned models in computational imaging: Theory, algorithms, and applications," *IEEE Signal Processing Magazine*, vol. 40, no. 1, pp. 85–97, 2023.

[29] K. Dabov, A. Foi, V. Katkovnik, and K. Egiazarian, "Image denoising by sparse 3-D transform-domain collaborative filtering," *IEEE Trans. Image Process.*, vol. 16, no. 8, pp. 2080–2095, 2007.

[30] A. Buades, B. Coll, and J.-M. Morel, "A review of image denoising algorithms, with a new one," *SIAM Multiscale Model. Simul.*, vol. 4, no. 2, pp. 490–530, 2005.

[31] A. Rond, R. Giryes, and M. Elad, "Poisson inverse problems by the plug-and-play scheme," *J. Vis. Commun. Image Represent.*, vol. 41, pp. 96–108, 2016.

[32] S.H. Chan, X. Wang, and O.A. Elgendy, "Plug-and-play admm for image restoration: Fixed-point convergence and applications," *IEEE Trans. Comput. Imaging*, vol. 3, no. 1, pp. 84–98, 2017.

[33] S. Dutta, A. Basarab, B. Georgeot, and D. Kouamé, "Plug-and-play quantum adaptive denoiser for deconvolving poisson noisy images," *IEEE Access*, vol. 9, pp. 139771–139791, 2021.

[34] X. Xu, Y. Sun, J. Liu, B. Wohlberg, and U.S. Kamilov, "Provable convergence of plug-and-play priors with mmse denoisers," *IEEE Signal Processing Letters*, vol. 27, pp. 1280–1284, 2020.

[35] S;H. Chan, "Performance analysis of plug-and-play admm: A graph signal processing perspective," *IEEE Trans. Comput. Imag.*, vol. 5, no. 2, pp. 274–286, 2019.

[36] S. Dutta, A. Basarab, B. Georgeot, and D. Kouamé, "Poisson image deconvolution by a plug-and-play quantum denoising scheme," in *Proc. 29th Eur. Signal Process. Conf. (EUSIPCO)*, 2021, pp. 646–650.

[37] Y. Chen and T. Pock, "Trainable nonlinear reaction diffusion: A flexible framework for fast and effective image restoration," *IEEE Trans. Pattern Anal. Mach. Intell.*, vol. 39, no. 6, pp. 1256–1272, 2017.

[38] K. Zhang, W. Zuo, Y. Chen, D. Meng, and L. Zhang, "Beyond a gaussian denoiser: Residual learning of deep CNN for image denoising," *IEEE Trans. Image Process.*, vol. 26, no. 7, pp. 3142–3155, 2017.

[39] K. Zhang, W. Zuo, and L. Zhang, "FFDNet: Toward a fast and flexible solution for cnn-based image denoising," *IEEE Trans. Image Process.*, vol. 27, no. 9, pp. 4608–4622, 2018.

[40] D. Yang and J. Sun, "BM3D-Net: A convolutional neural network for transform-domain collaborative filtering," *IEEE Signal Process. Lett.*, vol. 25, no. 1, pp. 55–59, 2018.

[41] M. Scetbon, M. Elad, and P. Milanfar, "Deep K-SVD denoising," *IEEE Trans. Image Process.*, vol. 30, pp. 5944–5955, 2021.

[42] S. Dutta, B. Georgeot, D. Kouamé, D. Garcia, and A. Basarab, "Adaptive contrast enhancement of cardiac ultrasound images using a deep unfolded many-body quantum algorithm," in *Proc. IEEE Int. Ultrason. Symp. (IUS)*, 2022, pp. 1–4.

[43] O. Féron, F. Orieux, and J.-F. Giovannelli, "Gradient scan gibbs sampler: An efficient algorithm for high-dimensional gaussian distributions," *IEEE J. Sel. Topics Signal Process.*, vol. 10, no. 2, pp. 343–352, 2016.

[44] J. Hatvani, A. Basarab, J.-Y. Tourneret, M. Gyöngy, and D. Kouamé, "A tensor factorization method for 3-d super resolution with application to dental ct," *IEEE Trans. Med. Imag.*, vol. 38, no. 6, pp. 1524–1531, 2019.

[45] Y. Romano, M. Elad, and P. Milanfar, "The little engine that could: Regularization by denoising (red)," *SIAM J. Imag. Sci.*, vol. 10, no. 4, pp. 1804–1844, 2017.

[46] S. Dutta, K.T. Nwigbo, J. Michetti, B. Georgeot, D.-H. Pham, A. Basarab, and D. Kouamé, "Quantum denoising-based super-resolution algorithm applied to dental tomography images," in *Proc. Int. Symp. Biomed. Imaging (ISBI)*, 2022, pp. 1–4.